Nano Energy 77 (2020) 105212

Contents lists available at ScienceDirect

Nano Energy

journal homepage: http://www.elsevier.com/locate/nanoen

Tensile-strained ruthenium phosphide by anion substitution for highly active and durable hydrogen evolution

Jianbing Zhu [a,1], Shuang Li [a,1], Meiling Xiao [a,1], Xiao Zhao [b], Gaoran Li [a], Zhengyu Bai [c], Matthew Li [a], Yongfeng Hu [d], Renfei Feng [d], Wenwen Liu [a], Rui Gao [a], Dong Su [e], Aiping Yu [a], Zhongwei Chen [a,*]

[a] Department of Chemical Engineering, Waterloo Institute for Nanotechnology, Waterloo Institute for Sustainable Energy, University of Waterloo, Waterloo, Ontario, Canada
[b] Innovation Research Center for Fuel Cells, The University of Electro-Communications, Chofu, Tokyo, 182-8585, Japan
[c] School of Chemistry and Chemical Engineering, Key Laboratory of Green Chemical Media and Reactions, Ministry of Education, Henan Normal University, Xinxiang, 453007, China
[d] Canadian Light Source, University of Saskatchewan, Saskatoon, Saskatchewan, S7N 0X4, Canada
[e] Beijing National Laboratory for Condensed Matter Physics, Institute of Physics, Chinese Academy of Sciences, Beijing, 100190, China

ARTICLE INFO

Keywords:
Ruthenium phosphide
Tensile strain
Anion substitution
Hydrogen evolution reaction
Electronic structure

ABSTRACT

Exploiting cost-effective, efficient and durable electrocatalysts toward hydrogen evolution reaction (HER) is of significant importance for the widespread application of water electrolyzers. Although ruthenium phosphide (RuP) has been hailed as a highly promising candidate, considerable performance disparity still lies between RuP and mainstream Pt/C benchmark, which calls for the structural regulation on RuP at molecular scale. Herein, for the first time, we develop a simple anion substitution strategy to obtain favorable strain regulation on RuP catalyst toward enhanced HER activity. The tensile strain enables an upshift of the d-orbital energy level of Ru site, facilitating hydrogen adsorption as well as water dissociation to accelerate the HER kinetics. Impressively, the as-developed N–RuP/NPC catalyst not only outperforms most of the reported Pt-free catalysts, showing record-high turnover frequencies of 1.56H_2 s^{-1} and 0.72H_2 s^{-1} at an overpotential of 30 mV in acidic and alkaline electrolyte, respectively, but also surpasses the Pt/C benchmark with a significantly smaller overpotential (58.9 mV vs 73.1 mV in acidic electrolyte) at a large current density of 100 mA cm^{-2}. Beyond that, such atomic level regulation also suppresses the electrochemical reconstruction and thereby guarantees superior durability over 10000 cycles.

1. Introduction

Efficient and cost-effective hydrogen mass production plays critical roles for sustainable social development [1]. Among the various strategies proposed, electrocatalytic water splitting has been recognized as a particularly attractive approach due to renewable source and zero carbon emission [2,3]. However, the widespread application of water electrolyzers has been obstructed by the exorbitant cost and scarcity of Pt-based electrocatalysts, which are indispensable to drive the kinetically-sluggish hydrogen evolution reaction (HER) at cathode [4]. Motivated by this challenge, the scientific community has been devoted to developing affordable and reliable substitutes during the past few decades [5–9]. Transition metal phosphides (TMPs) are recently emerging as a promising candidate for HER catalysis in both acidic and alkaline media, owing to their relatively low cost and promising catalytic activity [8–14]. Pioneered by the early work on hollow nickel phosphide [15], enormous efforts have been focused on tailoring the catalytic behaviors of TMPs to rival Pt involving a variety of strategies such as vacancy/morphology engineering [16–20], conductive substrate integration [21–24], heterogenous interface manipulation [25–30], etc. And very recently, ruthenium phosphide (RuP) has been found more active to catalyze HER than the first-row-transition-metal phosphides [12,31,32]. Notably, the price of Ru is ca. 25 times cheaper than Pt, affording potentially commercial application of Ru-based catalysts.

* Corresponding author.
E-mail address: zhwchen@uwaterloo.ca (Z. Chen).
[1] These authors contributed equally to this work.

https://doi.org/10.1016/j.nanoen.2020.105212
Received 4 June 2020; Received in revised form 6 July 2020; Accepted 21 July 2020
Available online 14 August 2020

Despite the encouraging progress, considerable performance disparity still lies between RuP and Pt benchmark, mainly ascribed to the unsatisfactory adsorption-desorption behaviors. Besides, RuP-based composites are also criticized by their insufficient stability as a result of multi-component or structural deficiency aroused by the aforementioned strategies. These inferiorities call for more sophisticated and effective strategies to more precisely structural regulation toward highly active and durable RuP catalyst.

Surface strain regulation is hailed as a powerful approach to tailor the catalytic properties by electronic modulation effect, however, the lack of efficient methodology is restricting the current research progress to specific catalysts with either core-shell heterointerfaces or 2D architecture, while rare advances have been achieved on the plain nanoparticulate catalysts [33,34]. Herein, we for the first time imposed a tensile strain on the RuP nanoparticles through a simple anion substitution method toward boosted hydrogen electrocatalysis (Scheme 1). The partial substation of P with N heteroatoms exerts internal stress on the RuP surface, inducing lattice distortion with expanded Ru–P bond. The resultant tensile strain in turn weakens the hybridization interaction between Ru 3d orbital and P 2p orbital and thereby leads to narrowed d-band of Ru site. As a result, such electronic-structure variation on the strained Ru site promotes hydrogen adsorption and water dissociation, therefore accelerating HER kinetics in both acidic and alkaline electrolytes. Benefiting from the structural merits, the as-developed N-doped RuP (N–RuP) nanoparticles exhibit admirable HER activity with minimum overpotentials at 100 mA cm^{-2} (58.9 in 0.5 M H_2SO_4 and 89.3 mV in 1 M KOH) and extremely high turnover frequency (TOF, 1.56 in 0.5 M H_2SO_4 and 0.72 in 1 M KOH at overpotential of 30 mV), outperforming the state-of-the-art Pt/C catalyst.

2. Materials and methods

2.1. Preparation of N–RuP/NPC

The ruthenium-melamine–diphenylphosphinic acid complex crystals with were synthesized by a wet chemistry method. Typically, 20 mmol melamine (2.52 g), 5 mmol diphenylphosphinic acid (1.09 g) and ultrapure water (100 mL) were added into a 250 mL single-necked, round-bottomed flask. Then flask was transferred into an oil bath and heated at 100 °C under stirring. After the solution became clear, a certain amount of $RuCl_3 \bullet xH_2O$ (0.12 mmol, 23.2 mg) and $ZnCl_2$ (3.67 mmol, 500 mg) was added into the solution and the mixture was allowed to react at 100 °C for 3 h. Finally, the solution was cooled down and frozen dry to obtain the precursor. The as-prepared precursor was placed in a quartz boat and then pyrolyzed at 1100 °C under argon atmosphere for 1 h with a heating rate of 2 °C/min.

2.2. Physical characterization

Scanning electron microscopy (SEM) measurements were performed with a LEO FESEM 1530 field emission scanning electron microscope. Transmission electron microscopy (TEM), high resolution transmission electron microscopy (HRTEM), high-annular dark-field scanning transmission electron microscopy (STEM) and element mapping analysis were conducted on TEM, JEOL 2010F. X-ray diffraction (XRD) measurements were performed with a Rigaku Miniflex 600 diffractometer using a Cu Kα (λ = 1.5405 Å) radiation source. To collect Raman spectra, a 532 nm laser source was employed. The Thermal Scientific Kα spectrometer was used to collect XPS spectra. Synchrotron powder X-ray diffraction (SP-XRD) measurements were conducted at the VESPERS (07B2-1) beamline, Canadian Light Source (CLS). The Ru K-edge were acquired in fluorescence mode using a Si (111) double-crystal monochromator and a 21 Ge-element detector for fluorescent X-rays at the BL36XU station in SPring-8. The EXAFS raw data were then background-subtracted, normalized and Fourier transformed by the standard procedures with the IFEFFIT package.

2.3. Electrochemical measurement

The activity for the HER was subsequently tested by LSV in nitrogen saturated 0.5 M H_2SO_4 or 1 M KOH solution with a scan rate of 5 mV s^{-1} and the data were iR compensated (95% iR compensated). Stability was investigated by continuous potential cycling in nitrogen-saturated electrolyte with a scan rate of 100 mV s^{-1}. And after 10,000 cycles, the HER steady-state polarization measurements were conducted in N_2-saturated electrolyte solution with scanning rates of 5 mV s^{-1}. CA measurements were conducted with the potential holding at −0.03 V at a rotating rate of 1600 rpm for 20 h. Commercial Pt/C (28 wt% Pt/C, TKK) catalyst were also measured for comparison. In all figures, the potentials were converted to values versus the reversible hydrogen electrode (RHE).

3. Results and discussion

The synthesis of N–RuP/NPC was accomplished via the direct pyrolysis of self-assembled melamine–diphenylphosphinicacid-ruthenium

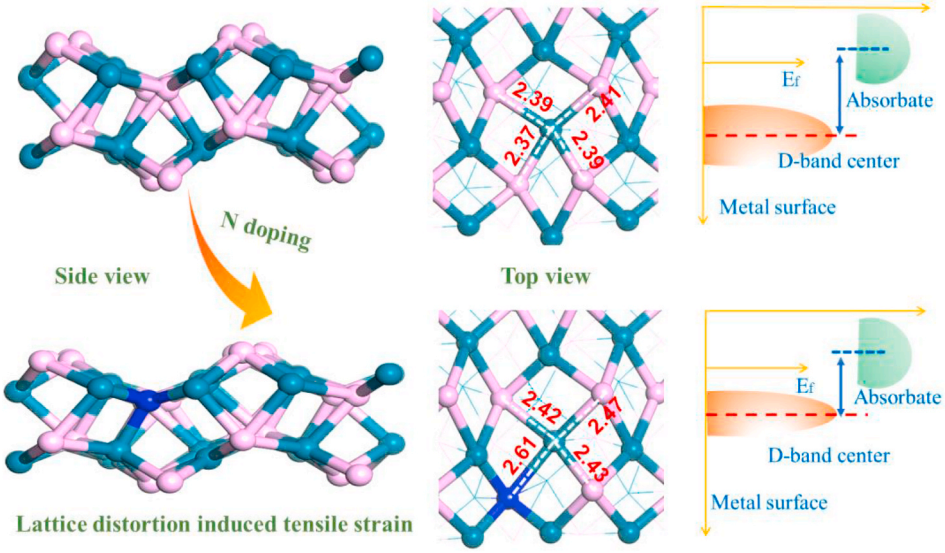

Scheme 1. Schematic illustration for the design of N-doped RuP with tailored electronic structure.

complex crystals (MDPR). Typically, melamine, diphenylphosphinicacid and ruthenium (III) acetylacetonate were firstly allowed to cooperatively assemble as reported in our previous work [35]; afterwards, the resultant MDPR nanobelts (Fig. S1) were subject to annealing under Ar atmosphere at 1100 °C to obtain the final N–RuP/NPC catalyst. Upon the preparation, a three-dimensional (3D) porous carbon architecture was achieved as a platform for anchoring the N-doped RuP nanoparticle toward uniform dispersion and easy access to catalytic sites. The control samples, including N, P dual doped carbon (NPC)-supported RuP nanoparticles (RuP/NPC) and Ru nanoparticles (Ru/NPC), were also prepared for comparative study (see details in Supplementary Information).

The crystal structures of the products were studied by X-ray diffraction (XRD). Both N–RuP/NPC and RuP/NPC display predominant diffraction peaks at 31.9°, 44.3° and 46.2°, corresponding to the (011), (112) and (211) planes of the orthorhombic RuP (JCPDS No. 34–0333), respectively, in sharp contrast to the typical metallic Ru peaks (JCPDS No. 65–7645) in Ru/NPC spectrum (Fig. 1a). Notably, a negative shift of the (011) peak can be discerned in the pattern of N–RuP/NPC compared with that of RuP/NPC, implying that N doping would expand the crystal lattice of RuP with an increase of ca. 0.2 Å in [011] direction (Fig. 1b). Synchrotron powder Bragg X-ray diffraction patterns also confirmed the enlarged lattice of RuP after N doping (Fig. S2). In addition to the set of metal/metal phosphide peaks, a broad peak at ~25° assigned to (002) plane of graphitic carbon is also observed in the XRD patterns, suggesting the presence of defective carbons. This is in line with the relatively large I_D/I_G value in the Raman spectra (Fig. S3 and Table S1). These defects not only serve as anchor sites for metal/metal phosphide particle deposition, but also exert electronic modulation effect to synergistically promote catalytic activity of the supported particles [36].

The microstructures were examined by scanning electron microscopy (SEM) and transmission electron microscope (TEM). The SEM image (Fig. S4) shows the similar 3D porous architecture assembled by carbon nanosheet for N–RuP/NPC, RuP/NPC and Ru/NPC. The surface

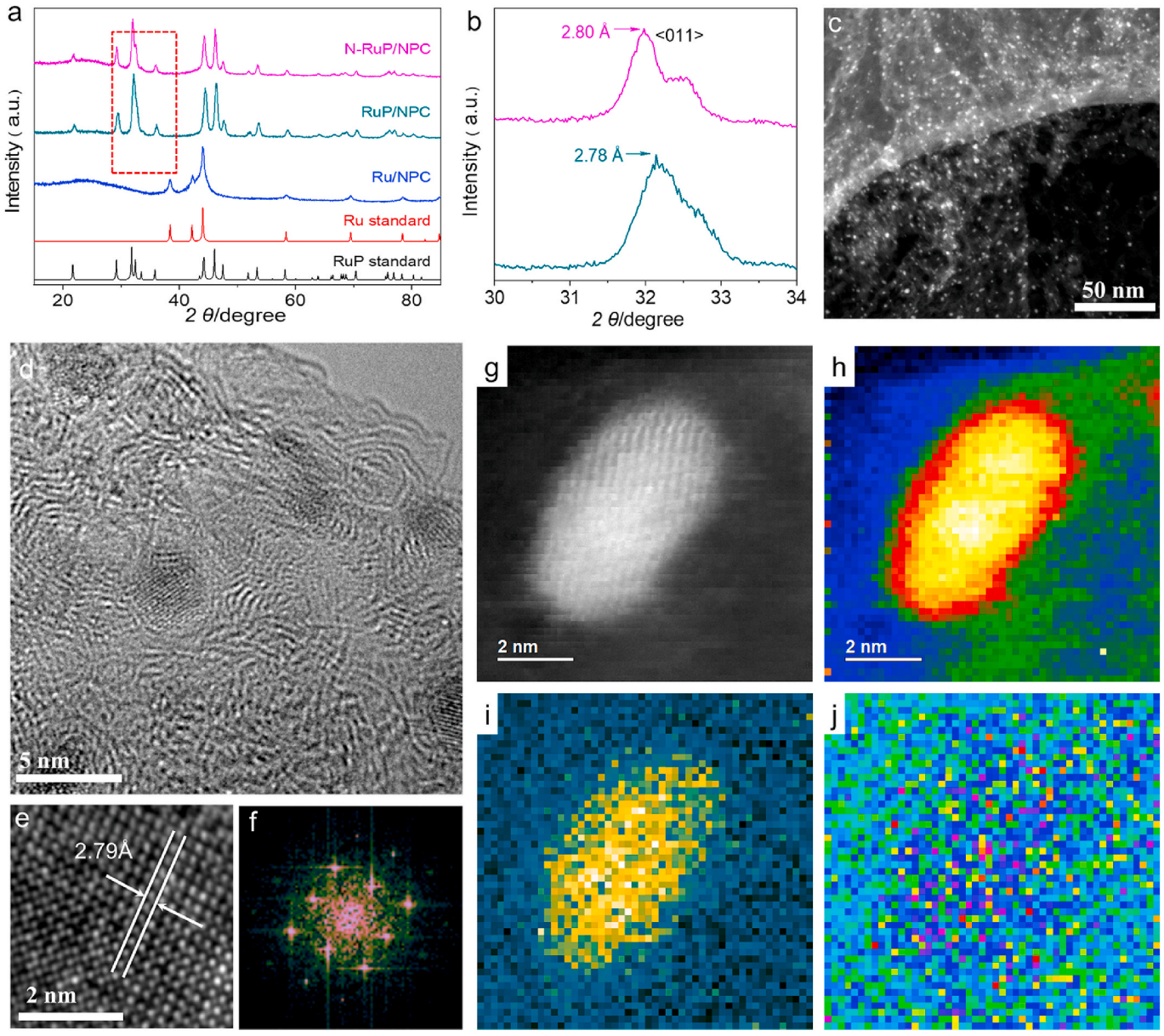

Fig. 1. (a) Powder XRD pattern of N–RuP/NPC; (b) SEM image of N–RuP/NPC catalyst revealing its graphene-like morphology; (c) STEM image of N–RuP/NPC; (d) HRTEM image of the N–RuP/NPC catalyst; (e) magnified HRTEM image of the N–RuP/NPC catalyst; (f) corresponding FFT pattern of (e); (g–j) HAADF STEM image and corresponding EELS elemental mapping of N–RuP/NPC catalyst, (g) HAADF image of N–RuP/NPC; (h) overlap EELS elemental mapping; (i) P K-edge; (j) N K-edge.

area of N–RuP/NPC was determined ca. 960 $m^2 g^{-1}$ as shown in Fig. S5. This interconnected and porous nanostructure is favorable for active site exposure and electron/mass transfer in the electrocatalytic process, thereby representing an ideal catalytic platform. The uniformly dispersed N–RuP nanoparticles with a mean size of ca. 2.28 nm can be clearly discerned in the high-angle annular dark-field scanning transmission electron microscopy (HAADF-STEM) image (Fig. 1c and S6). Similarly, both RuP/NPC (Fig. S7) and Ru/NPC (Fig. S8) also exhibit fine nanoparticles with good crystallinity. Such a small particle size benefits from the strong metal-support interaction, where the rich defects and functionalities in the substrate suppress the Ostwald ripening at high annealing temperature. The permeation of N dopants into the RuP lattice was confirmed by electron energy loss spectroscopy (Fig. 1g–j), where the Ru, P, and N elements distribute homogenously in a single RuP particle. By contrast, N signals predominately present in the carbon matrix rather than RuP particle for the RuP/NPC sample (Fig. S7e-h). A

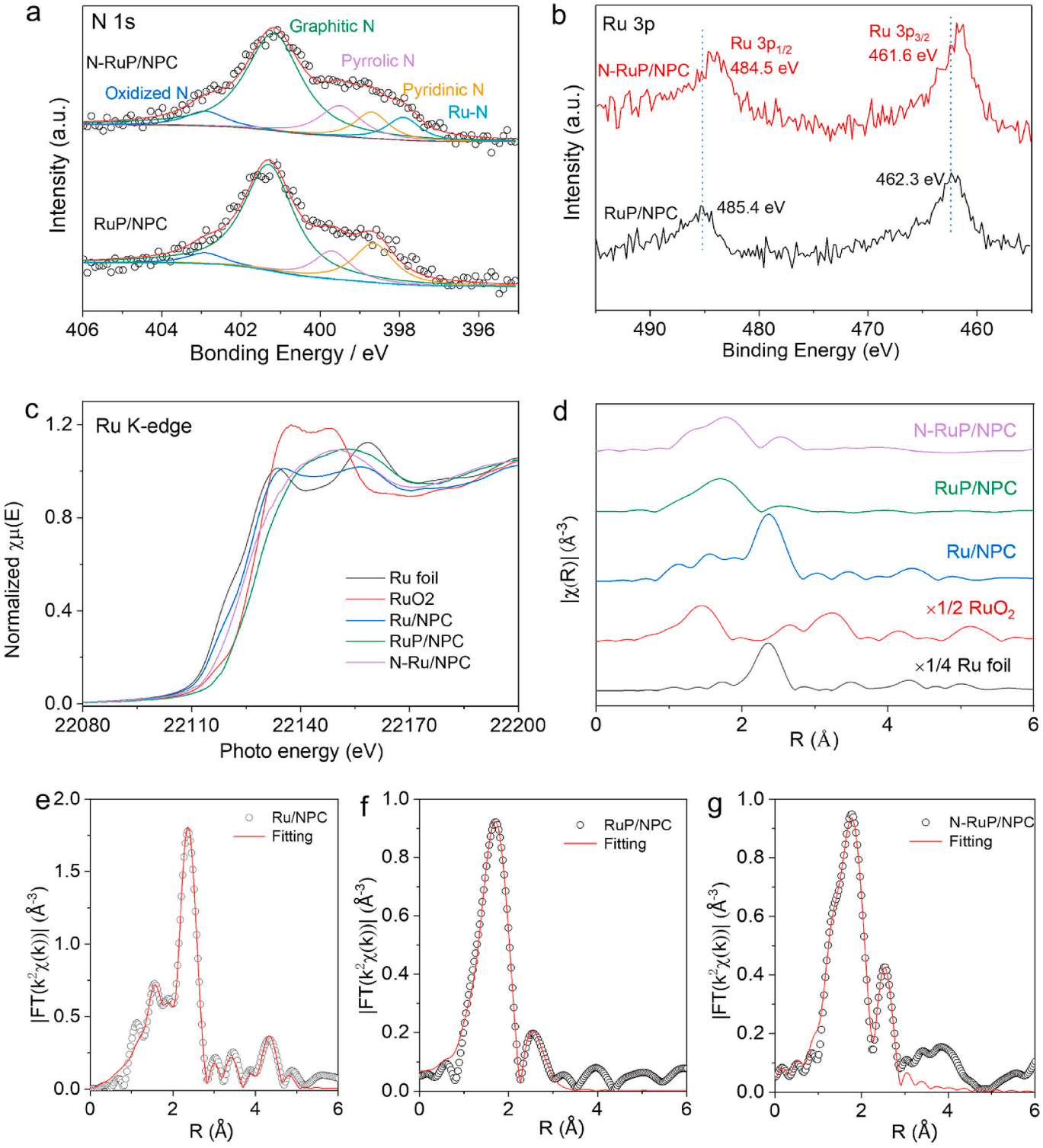

Fig. 2. (a) High-resolution N 1s XPS spectra, (b) Ru 3p XPS spectra for N–RuP/NPC and RuP/NPC (c) Ru K-edge XANES spectra and (d) Fourier transforms of k3-weighted Ru K-edge EXAFS data for commercial Ru foil, RuO2 and N–RuP/NPC; (e–g) fitting results of FT-EXAFS for (e) Ru/NPC, (f) RuP/NPC and (g) N–RuP/NPC.

larger lattice fringes of (011) plane is observed in the HRTEM image and the corresponding FFT patterns for N–RuP/NPC (2.79 Å vs 2.76 Å for RuP/NPC), in line with the negative shift of (011) peak in the XRD patterns. These results suggest that the N doping into RuP leads to a lattice distortion, and promisingly trigger the tensile or compressive strain.

Further evidence for the N doping and the resultant strain effect was gained by investigating the local atom arrangement and the electronic structure. The surface composition and chemical states were examined by X-ray photoelectron spectroscopy (XPS, Fig. 2a and b, Fig. S9–11 and Table S2). As illustrated in Fig. 2a, a typical Ru–N peak (397.9 eV) can be deconvoluted in the high-resolution N 1s XPS spectrum of N–RuP/NPC in addition to the oxidized N (402.9 eV), graphitic N (401.2 eV), pyrrolic N (399.5 eV) and pyridinic N (398.7 eV). By contrast, this peak is absent in the spectra of RuP/NPC, Ru/NPC and NPC (Fig. 2a, Fig. S10b and S11b). Meanwhile, both the P 2p XPS spectra of N–RuP/NPC and RuP/NPC (Fig. S8b and S8d) display predominant peaks of P–O (133.6 eV), P–C (132.3 eV) and P–Ru (130.9 eV and 129.9 eV). The presence of Ru–N and absence of P–N peaks in the N–RuP/NPC spectra suggest that N prefers to substitutes the P site rather than the Ru site, which is speculated to decrease the electronic density of the adjacent Ru atoms due to the higher electronegativity of N than P. Interestingly, the Ru 3p peaks shift negatively after N doping (Fig. 2b), indicating the increased electronic density. Besides, such effect can be also perceived from the X-ray absorption near edge spectroscopy (XANES), where a slight negative shift in absorption energy and a lower white-line intensity can be observed in the Ru K-edge spectrum of N–RuP/NPC compared with that of RuP/NPC (Fig. 2c and S12), confirming the enriched electronic density of Ru. These contradictive results imply another mechanism against the general electronic modulation by ligand effect of N as dominatingly reported in literatures. Combining with the lattice expansion observed in the aforementioned analysis, the mechanism is expected to be tensile strain effect.

Given this, extended X-ray absorption fine structure spectroscopy (EXAFS) was carried out to provide more detailed information on the local configuration around Ru atoms. All the data presented in the EXAFS spectra are not phase corrected. In the Fourier transforms (FT) of EXAFS spectra (Fig. 2d), both RuP/NPC and N–RuP/NPC exhibit two main peaks at ~2.5 Å and ~1.7 Å attributed to the Ru–Ru and Ru–P/N scattering path, respectively, while the Ru/NPC benchmark displays a dominant Ru–Ru path at ~2.35 Å. Notably, the first-shell peak shifts to higher R in the spectrum of N–RuP/NPC, revealing a larger Ru–P/N

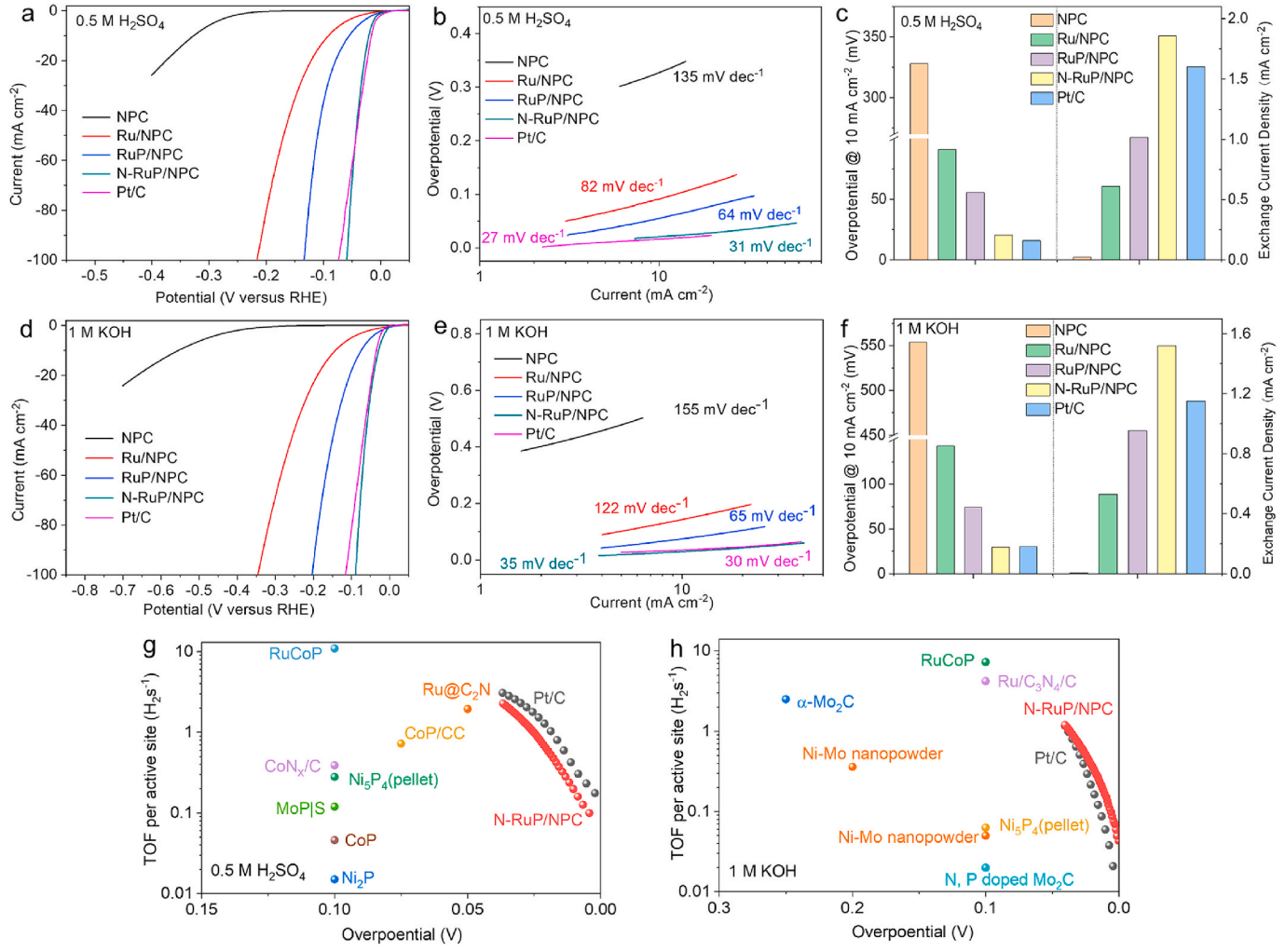

Fig. 3. (a) LSV polarization curves of N–RuP/NPC, RuP/NPC, Ru/NPC, NPC and commercial Pt/C catalysts in 0.5 M H_2SO_4 solution at a scan rate of 5 mV s^{-1} with an electrode rotation speed of 1600 rpm; (b) Tafel plots derived from the LSV polarization curves in (a); (c) comparison of overpotential at 10 mA cm^{-2} (left) and exchange current densities (right) of N–RuP/NPC, RuP/NPC, Ru/NPC, NPC and commercial Pt/C catalysts in 0.5 M H_2SO_4 solution; (d) LSV polarization curves of N–RuP/NPC, RuP/NPC, Ru/NPC, NPC and commercial Pt/C catalysts in 1 M KOH solution at a scan rate of 5 mV s^{-1} with an electrode rotation speed of 1600 rpm; (e) Tafel plots derived from the LSV polarization curves in (d); (f) Comparison of overpotential at 10 mA cm^{-2} (left) and exchange current densities (right) of N–RuP/NPC, RuP/NPC, Ru/NPC, NPC and commercial Pt/C catalysts in 1 M KOH solution, (g, h) Comparison of TOF values of the N–RuP/NPC and Pt/C with other recently reported HER electrocatalysts: (g) in acidic medium; (h) in alkaline medium.

bond length. The best-fitting analysis of FT-EXAFS (Fig. 2e–f and Fig. S13 and Table S3) further validates the enlarged Ru–P bond (2.37 Å) with a coordination number of less than 4.5. By contrast, the Ru–P bond length in the pristine RuP/NPC is estimated to be 2.32 Å with a coordination number of 5.3. The enlarged Ru–P bond length and decreased Ru–P coordination number provide direct evidence for the tensile strain induced by partial N substitution. As a result, the tensile strain would weaken the hybridization interaction between Ru 3d orbital and P 2p orbital and thereby results in narrowed d-band of Ru site, which in turn beneficially regulates the adsorption-desorption behaviors on the Ru site toward boosted catalytic activity.

In view of the tailored electronic structure by tensile strain, the HER electrocatalytic performance of the as-prepared catalysts was examined firstly in 0.5 M H_2SO_4 solution in comparison with commercial Pt/C benchmark. The linear sweep voltammetry (LSV) curves (Fig. 3a) reveal an onset overpotential (E_{onset}) of ca. 0 mV for N–RuP/NPC to trigger the HER, which is similar to that of the commercial Pt/C; whereas the E_{onset} for RuP/NPC, Ru/NPC and NPC turn out to be 5, 22, and 237 mV, respectively. The lowest E_{onset} on N–RuP/NPC suggests its highest intrinsic activity among these samples. Moreover, the overpotential for approaching the current density of 10 mA cm^{-2} is measured to be 20.5 mV on N–RuP/NPC, much lower than those of RuP/NPC (55.6 mV), Ru/NPC (91.1 mV), NPC (328.1 mV) counterparts and also superior to most of the reported Pt-free catalysts (Table S4). More commendably, the N–RuP/NPC also outperforms the Pt/C benchmark at large current region with a remarkably smaller overpotential (58.9 vs. 73.1 mV at 100 mA cm^{-2}), demonstrating the promising practical application of N–RuP/NPC in water electrolyzers. The superior HER activity of N–RuP/NPC was further verified by its extraordinary lower Tafel slope of 31 mV dec^{-1} than that of RuP/NPC (64 mV dec^{-1}), Ru/NPC (82 mV dec^{-1}) and NPC (135 mV dec^{-1}), implying the faster HER kinetics on N–RuP/NPC (Fig. 3b). This result also suggests that the HER pathway follows Volmer-Tafel mechanism, where the rate-determining step is the recombination of the chemisorbed hydrogen atoms (Tafel reaction). Furthermore, the exchange current density (j_0), which is regarded as an indicator for the intrinsic activity, was obtained by extrapolating the Tafel plots (Fig. 3c). Impressively, the j_0 reaches as high as 1.86 mA cm^{-2} on N–RuP/NPC, surpassing the RuP/NPC (1.02 mA cm^{-2}) and the Pt/C benchmark (1.61 mA cm^{-2}). The significant enhancement in HER activity of N–RuP/NPC is attributed to ameliorative electronic structure induced by tensile strain effect, which in turn results in optimized adsorption-desorption behaviours of reaction intermediates on the strained active site.

The HER performance was further examined in 1 M KOH solution. Although the HER reaction rate in alkaline electrolyte is generally considered 2–3 orders of magnitude lower than that in acidic medium, the as-developed N–RuP/NPC retains its excellent catalytic activity in 1 M KOH solution (Fig. 3d). Specifically, N–RuP/NPC exhibits an overpotential of 29.6 mV to drive a catalytic current of 10 mA cm^{-2}, which not only outperforms the RuP/NPC (74.3 mV), Ru/NPC (143.1 mV) and NPC (553.9 mV), but also surpasses the Pt/C benchmark (30.5 mV). Moreover, the N–RuP/NPC is also superior to most of the HER catalysts in recent reports in terms of the relatively lower overpotential at 10 mA cm^{-2} (Table S5). Even at higher current densities of 20, 50 and 100 mA cm^{-2}, the N–RuP/NPC catalyst only requires small overpotentials of 42, 66 and 89 mV, respectively, superior to those of other counterparts. The accelerated HER kinetics on N–RuP/NPC in alkaline electrolyte can be further verified by Tafel analysis. As shown in Fig. 3e, N–RuP/NPC shows a comparable Tafel slope of 35 mV dec^{-1} to commercial Pt/C (30 mV dec^{-1}), which is much lower than those of the other samples, revealing that the tensile strain effect facilities the water dissociation and thus accelerates the hydrogen adsorption process (Volmer step: $H_2O + e^- \leftrightarrow H_{ad} + OH^-$). Meanwhile, the j_0 of N–RuP/NPC is estimated to be 1.52 mA cm^{-2}, corresponding to 1.6-fold enhancement compared with RuP/NPC, which further manifests the superiority of the tensile strained site (Fig. 3f).

To further demonstrate the advantages of the strained N–RuP site quantitatively, the turnover frequency (TOF), which represents the intrinsic electrocatalytic activity of per active site, was calculated in comparison with the recently reported representative HER electrocatalysts in both acidic and alkaline solutions (Fig. S14-S16, Table S4 and S5). As shown in Fig. 3g, N–RuP/NPC displays an admirable TOF of 1.16H_2 s^{-1} and 4.52H_2 s^{-1}, at 25 mV and 50 mV, respectively, surpassing the generally recognized transition metal dichalcogenides and phosphides, i.e., MoS_2 [37], CoP [38], Ni_2P [15], MoP|S [39], CoNx/C [40], Ni_5P_4 (pellet) [41], CoP/CC [17], RuCoP [42] and Ru@C_2N [43], in 0.5 M H_2SO_4. The much higher TOF of N–RuP/NPC suggests increased intrinsic activity as a result of the well-designed energy level of RuP by tensile strain effect. More delightfully, satisfactory TOF was found to be retained on the N–RuP/NPC in 1.0 M KOH. Specifically, the TOF values of N–RuP/NPC in 1.0 M KOH solution were 1.85H_2 s^{-1} at the overpotentials of 50 mV, larger than that of Pt/C (1.66H_2 s^{-1}) and far exceeds the reported alternatives, α-Mo_2C [44], Ni-Mo Nanopowder [45], Ni_5P_4 (pellet) [41], N, P doped Mo_2C [46], RuCoP [42] and Ru/C_3N_4/C [47] (Fig. 3h and Table S5). The ultra-high TOF values in both acidic and alkaline solutions suggest the successful electronic modulation on the RuP active site for boosted HER activity, and the as-developed N–RuP/NPC can serve as a promising candidate to replace Pt in water splitting.

In addition to activity, stability is another important criterion for electrocatalyst evaluation, especially for practical application. Accordingly, the accelerated durability test (ADT) and time-dependent chronopotentiometric (CP) measurements were carried out to investigate the electrocatalytic stability of N–RuP/NPC. After continuous 10,000 cycling in 0.5 M H_2SO_4, the polarization curve of N–RuP/NPC presents slight negative shift of 5.2 mV at the current density of 10 mA cm^{-2}, superior to the Ru/NPC and RuP/NPC counterparts (Fig. 4a and Fig. S17). Besides, there is only slight current fluctuation within 20 h operation under a fixed overpotential of 30 mV (insert Fig. 4a). By contrast, the Pt/C benchmark exhibits a larger activity decay with 13.7 mV positive shift after the ADT test. Apart from that, the stability test in alkaline electrolyte also reveals enhanced long-term durability of N–RuP/NPC compared with the RuP/NPC counterpart with a negligible degradation during the long period of cycling (Fig. 4b and c, Fig. S18). The excellent stability of N–RuP/NPC is probably due to the strong metal-support interaction, which prohibits the aggregation/detachment of nanoparticles during electrochemical process. Additionally, the hierarchically porous structure promotes the gas diffusion to avoid blocking the active sites.

Considering the excellent activity and stability of N–RuP/NPC in both acidic and alkaline electrolytes, we further evaluated the overall water splitting activity in a two-electrode configuration by employing N–RuP/NPC and IrO_2 as cathode and anode, respectively (Fig. 4d). Pt/C was also utilized as cathode for comparative study. As depicted in Fig. 4e, N–RuP/NPC||IrO_2 exhibits superior acidic water splitting performance with a preferably low cell voltage of 1.677 V to reach a current density of 50 mA cm^{-2}, which is 23 mV lower than that of Pt/C||IrO_2 (1.70 V, Fig. S19). Beyond that, the cell performance in 1 M KOH was investigated as well. Excitingly, the device is capable to deliver a current density of 50 mA cm^{-2} at an operating voltage of 1.73 V, outperforming the Pt/C||IrO_2 benchmark (1.76 V, Fig. S19). Furthermore, the N–RuP/NPC||IrO_2 also possesses excellent long-term stability with only a 56 mV and 52 mV cell potential increase, in 0.5 M H_2SO_4 and 1 M KOH, respectively after 100 h continuous operation at 20 mA cm^{-2} (Fig. 4f). Based on these results, the as-developed N–RuP/NPC can serve as a highly promising candidate in practical water electrolysis applications.

To unveil the underlying mechanism of the unprecedented HER activity of N–RuP/NPC, we conducted density functional theory (DFT) calculations. First, charge distribution and density of states (DOS) were calculated to investigate the tensile strain effect on electronic structure. A local charge redistribution induced by N-doping was found in the charge difference diagram for the strained RuP surface (Fig. 5a and b). It can be perceived that electrons are enriched in the Ru atom (red circled)

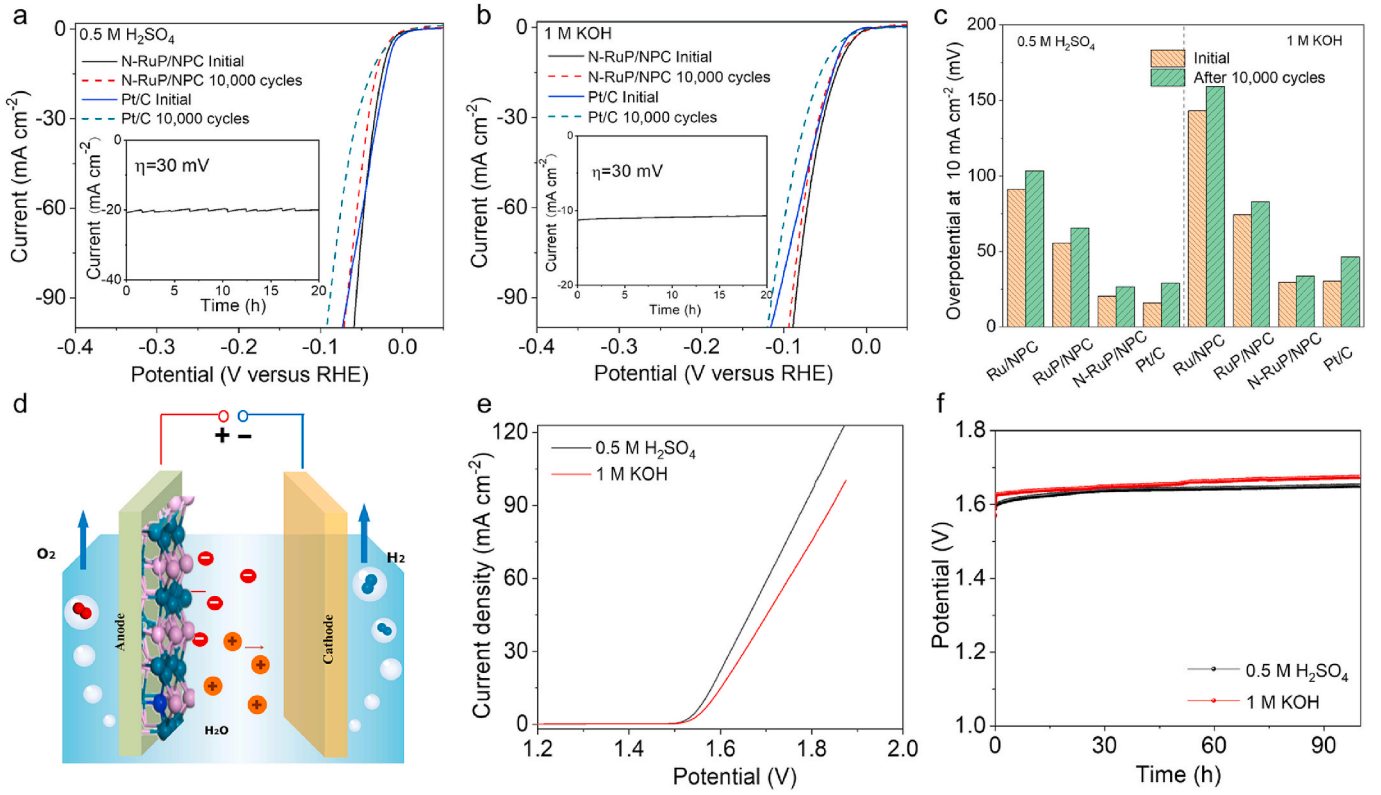

Fig. 4. (a) Stability tests of the N–RuP/NPC and Pt/C in 0.5 M H_2SO_4 solution before and after 10, 000 potential CV cycles at a scan rate of 5 mV s^{-1} with an electrode rotation speed of 1600 rpm, inset shows the i-t curve of N–RuP/NPC catalyst at an overpotential of 30 mV; (b) stability tests of the N–RuP/NPC and Pt/C in 1 M KOH solution before and after 10, 000 potential CV cycles at a scan rate of 5 mV s^{-1} with an electrode rotation speed of 1600 rpm, inset shows the i-t curve of N–RuP/NPC catalyst at an overpotential of 30 mV; (c) comparison of overpotential changes at 10 mA cm^{-2} after 10, 000 potential CV cycles in 0.5 M H_2SO_4 (left) and 1 M KOH (right) solutions; (d) schematic illustration of an electrolyzer with N–RuP as cathode and commercial IrO_2 as anode (N–RuP/NPC||IrO_2); (e) LSV polarization curves for overall water splitting of the N–RuP/NPC||IrO_2 couple in 0.5 M H_2SO_4 (black line) and 1 M KOH (red line); (f) chronopotentiometric curves recorded at a current density of 20 mA cm^{-2} in acidic (black line) and alkaline medium (red line).

due to the weakened electron transfer from Ru to the adjacent P atoms. Besides, more obvious d-orbital splitting was observed on the strained Ru site, which could in turn induce the spin polarization. As a result, the spin polarization in conjunction with charge polarization would promote the hydrogen adsorption. The d-band center, as a descriptor for the metal-absorbate binding strength, was further computed to verify the speculation. Impressively, the N–RuP exhibits a higher d-band center of −2.68 eV than RuP (−2.96 eV), suggesting the enhanced absorption energy of intermediates on the N–RuP site (Fig. 5c and d). The absorption-desorption behaviors were further examined on the catalyst surface (Fig. 5e and f). Since the Gibbs free energy of hydrogen adsorption (ΔG_{H^*}) is commonly regarded as an indicator in the theoretical prediction of the HER activity [48], the ΔG_{H^*} values on N–RuP and pristine RuP were calculated (Fig. 5g). In the pristine RuP structure, the ΔG_{H^*} value of the P site and Ru site is −0.007 and 0.246 eV, respectively, suggesting that the former site is more catalytically active to HER, while the weak binding strength of Ru–H on the later site is unfavorable for the Volmer step. After N doping, the ΔG_{H^*} value of the Ru site is dramatically decreased to −0.015 eV on the strained surface, implying an easier hydrogen adsorption process. Meanwhile, the P site retains the excellent intrinsic activity with a ΔG_{H^*} of 0.005 eV. These results reveal that the tensile strain induced by N doping activates Ru site and maintained P site simultaneously for achieving boosted HER activity in line with the experimental results in acidic electrolyte. Apart from that, the absorption energy of H_2O (E_{H2O}) on the catalysts was also computed to evaluate the HER activity in alkaline solution considering that the HER in alkaline media requires an additional first step of water dissociation (Fig. 5h–j). More negative E_{H2O} was found on the N–RuP (−0.468 eV) surface compared with RuP (−0.402 eV), implying a faster Volmer process on the N–RuP surface. Moreover, the O–H bond length was enlarged from 0.97 Å to 0.99 Å after N doping, further confirming the H_2O molecular preferred to dissociate into hydroxyl and H on the N–RuP surface. The above DFT calculations clearly verified that the tensile strain indeed tailors the electronic structure of RuP, which optimizes the hydrogen absorption energy on Ru site and facilitates the water dissociation, leading to improved HER activity.

4. Conclusion

In summary, we developed an advanced nanoparticulate RuP catalyst for highly active and durable hydrogen electrocatalysis. Morphology, composition and local environment characterizations demonstrate that doping N into RuP lattice induce tensile strain and thereby tailor the energy level of RuP. The as-obtained N–RuP/NPC requires remarkably low overpotential of 58.9 and 89.3 mV to reach the current density of 100 mA cm^{-2}, in acidic and alkaline electrolyte, respectively, outperforming most of the reported Pt-free catalysts and even the commercial Pt/C benchmark. Insights into the underlying mechanism were revealed by DFT calculations, which confirmed that the tensile strain effect can effectively upshift the d-band center of Ru and therefore enhances the H absorption and promotes the water dissociation, contributing to the high intrinsic activity of N–RuP/NPC. Our study not only introduces N–RuP/NPC as a promising HER catalyst for practical application, but also provide a methodology to tailor chemical/physical properties for desirable catalytic activity.

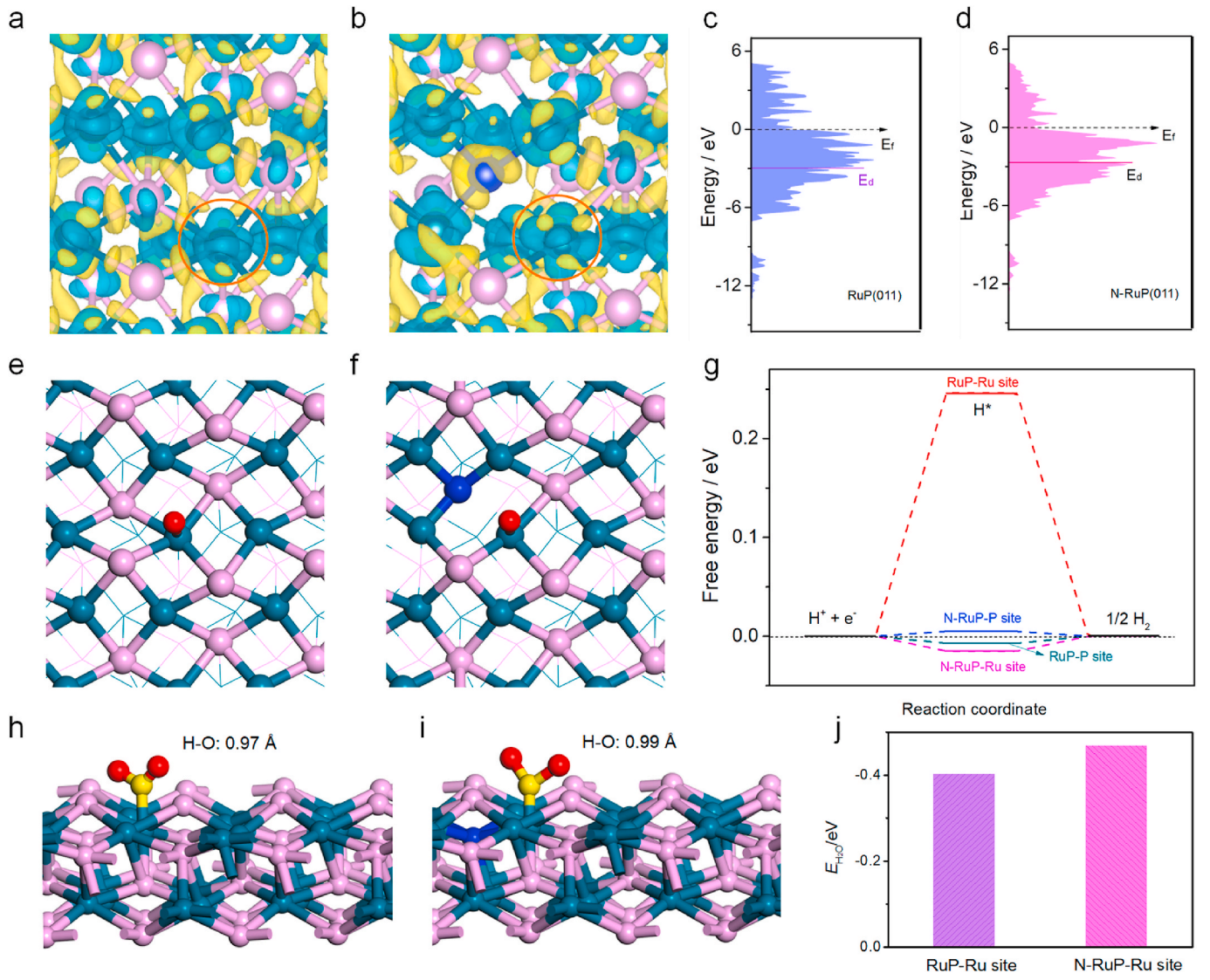

Fig. 5. Charge density difference for (a) RuP (011), (b) N–RuP (011), blue and yellow areas represent charge density decrease and increase, respectively; The calculated pDOS of Ru site for (c) RuP (011), (d) N–RuP (011); Optimized structures of H adsorption on (e) RuP (011)-Ru site, (f) N–RuP (011)-Ru site; (g) Gibbs free energy diagrams for HER; Optimized structures of H2O adsorption on (h) RuP (011)-Ru site, (i) N–RuP (011)-Ru site; (j) Adsorption energy of H2O on RuP (011)-Ru site and N–RuP (011)-Ru site. Ru (dark cyan), P (pink), N (blue), O (yellow), and H (red).

CRediT authorship contribution statement

Jianbing Zhu: Conceptualization, Methodology, Data curation, Writing - original draft, Visualization, Investigation, Validation, Writing - review & editing. **Shuang Li:** Conceptualization, Methodology, Data curation, Writing - original draft, Validation, Writing - review & editing. **Meiling Xiao:** Conceptualization, Methodology, Data curation, Writing - original draft, Validation, Writing - review & editing. **Xiao Zhao:** Data curation, Writing - original draft, Visualization, Investigation. **Gaoran Li:** Conceptualization, Data curation, Visualization, Writing - original draft, Writing - review & editing. **Zhengyu Bai:** Conceptualization, Data curation, Investigation, Writing - review & editing. **Matthew Li:** Visualization, Writing - original draft, Writing - review & editing. **Yongfeng Hu:** Methodology, Data curation, Writing - original draft. **Renfei Feng:** Methodology, Data curation, Writing - original draft. **Wenwen Liu:** Methodology, Data curation, Writing - original draft. **Rui Gao:** Methodology, Data curation, Writing - original draft. **Dong Su:** Conceptualization, Methodology, Writing - review & editing. **Aiping Yu:** Conceptualization, Methodology, Writing - review & editing. **Zhongwei Chen:** Conceptualization, Methodology, Supervision, Validation, Writing - review & editing.

Declaration of competing interest

The authors declare that they have no known competing financial interests or personal relationships that could have appeared to influence the work reported in this paper.

Acknowledgments

The authors would like to acknowledge the financial support from the University of Waterloo. The Catalysis Research for Polymer Electrolyte Fuel Cells (CaRPE FC) Network administered from Simon Fraser University and supported by Automotive Partnership Canada (APC) Grant no. APCPJ 417858–11 through the Natural Sciences and Engineering Research Council of Canada (NSERC) are greatly acknowledged. Electron microscopy work was performed at the Center for Functional Nanomaterials, Brookhaven National Laboratory, which is supported by the U.S. Department of Energy (DOE), Office of Basic Energy Science, under Contract No. DE-SC0012704. The authors also gratefully

acknowledge support from Canadian Light Sources (CLS) for XAS measurements. The CLS is supported by NSERC, the national Research Council Canada, the Canadian Institutes of Health Research, the Province of Saskatchewan, Western Economic Diversification Canada, and the University of Saskatchewan.

Appendix A. Supplementary data

Supplementary data related to this article can be found at https://doi.org/10.1016/j.nanoen.2020.105212.

References

[1] S. Chu, A. Majumdar, Nature 488 (2012) 294–303.
[2] L.M. Gandía, R. Oroz, A. Ursúa, P. Sanchis, P.M. Diéguez, Energy Fuels 21 (2007) 1699–1706.
[3] R. Subbaraman, D. Tripkovic, D. Strmcnik, K.-C. Chang, M. Uchimura, A. P. Paulikas, V. Stamenkovic, N.M. Markovic, Science 334 (2011) 1256–1260.
[4] A.R. Zeradjanin, J.-P. Grote, G. Polymeros, K.J.J. Mayrhofer, Electroanalysis 28 (2016) 2256–2269.
[5] Z. Luo, Y. Ouyang, H. Zhang, M. Xiao, J. Ge, Z. Jiang, J. Wang, D. Tang, X. Cao, C. Liu, W. Xing, Nat. Commun. 9 (2018) 2120.
[6] W. Ahn, M.G. Park, D.U. Lee, M.H. Seo, G. Jiang, Z.P. Cano, F.M. Hassan, Z. Chen, Adv. Funct. Mater. 28 (2018) 1802129.
[7] B. Hinnemann, P.G. Moses, J. Bonde, K.P. Jørgensen, J.H. Nielsen, S. Horch, I. Chorkendorff, J.K. Nørskov, J. Am. Chem. Soc. 127 (2005) 5308–5309.
[8] P. Xiao, W. Chen, X. Wang, Adv. Energy Mater. 5 (2015) 1500985.
[9] Y. Shi, B. Zhang, Chem. Soc. Rev. 45 (2016) 1529–1541.
[10] J. Kibsgaard, C. Tsai, K. Chan, J.D. Benck, J.K. Nørskov, F. Abild-Pedersen, T. F. Jaramillo, Energy Environ. Sci. 8 (2015) 3022–3029.
[11] J.F. Callejas, C.G. Read, C.W. Roske, N.S. Lewis, R.E. Schaak, Chem. Mater. 28 (2016) 6017–6044.
[12] J. Yu, Y. Guo, S. She, S. Miao, M. Ni, W. Zhou, M. Liu, Z. Shao, Adv. Mater. 30 (2018) 1800047.
[13] P. Xiao, M.A. Sk, L. Thia, X. Ge, R.J. Lim, J.-Y. Wang, K.H. Lim, X. Wang, Energy Environ. Sci. 7 (2014) 2624–2629.
[14] Y. Yan, B.Y. Xia, X. Ge, Z. Liu, A. Fisher, X. Wang, Chemistry–Eur. J. 21 (2015) 18062–18067.
[15] E.J. Popczun, J.R. McKone, C.G. Read, A.J. Biacchi, A.M. Wiltrout, N.S. Lewis, R. E. Schaak, J. Am. Chem. Soc. 135 (2013) 9267–9270.
[16] Z. Zhang, J. Hao, W. Yang, J. Tang, ChemCatChem 7 (2015) 1920–1925.
[17] J. Tian, Q. Liu, A.M. Asiri, X. Sun, J. Am. Chem. Soc. 136 (2014) 7587–7590.
[18] X.-D. Wang, Y.-F. Xu, H.-S. Rao, W.-J. Xu, H.-Y. Chen, W.-X. Zhang, D.-B. Kuang, C.-Y. Su, Energy Environ. Sci. 9 (2016) 1468–1475.
[19] Q. Fu, T. Wu, G. Fu, T. Gao, J. Han, T. Yao, Y. Zhang, W. Zhong, X. Wang, B. Song, ACS Energy Lett. 3 (2018) 1744–1752.
[20] J. Chang, S. Li, G. Li, J. Ge, C. Liu, W. Xing, J. Mater. Chem. 4 (2016) 9755–9759.
[21] Q. Liu, J. Tian, W. Cui, P. Jiang, N. Cheng, A.M. Asiri, X. Sun, Angew. Chem. Int. Ed. 53 (2014) 6710–6714.
[22] G. Li, Y. Sun, J. Rao, J. Wu, A. Kumar, Q.N. Xu, C. Fu, E. Liu, G.R. Blake, P. Werner, B. Shao, K. Liu, S. Parkin, X. Liu, M. Fahlman, S.-C. Liou, G. Auffermann, J. Zhang, C. Felser, X. Feng, Adv. Energy Mater. 8 (2018) 1801258.
[23] Y. Shi, Y. Xu, S. Zhuo, J. Zhang, B. Zhang, ACS Appl. Mater. Interfaces 7 (2015) 2376–2384.
[24] Y. Yang, M. Luo, Y. Xing, S. Wang, W. Zhang, F. Lv, Y. Li, Y. Zhang, W. Wang, S. Guo, Adv. Mater. 30 (2018) 1706085.
[25] M. Cabán-Acevedo, M.L. Stone, J.R. Schmidt, J.G. Thomas, Q. Ding, H.-C. Chang, M.-L. Tsai, J.-H. He, S. Jin, Nat. Mater. 14 (2015) 1245.
[26] T. Zhang, K. Yang, C. Wang, S. Li, Q. Zhang, X. Chang, J. Li, S. Li, S. Jia, J. Wang, L. Fu, Adv. Energy Mater. 8 (2018) 1801690.
[27] X. Liu, Q. Hu, B. Zhu, G. Li, L. Fan, X. Chai, Q. Zhang, J. Liu, C. He, Small 14 (2018) 1802755.
[28] T. Liu, A. Li, C. Wang, W. Zhou, S. Liu, L. Guo, Adv. Mater. 30 (2018) 1803590.
[29] R. Boppella, J. Tan, W. Yang, J. Moon, Adv. Funct. Mater. 29 (2019) 1807976.
[30] J. Chang, Q. Lv, G. Li, J. Ge, C. Liu, W. Xing, Appl. Catal. B Environ. 204 (2017) 486–496.
[31] Z. Pu, I.S. Amiinu, Z. Kou, W. Li, S. Mu, Angew. Chem. Int. Ed. 56 (2017) 11559–11564.
[32] Q. Qin, H. Jang, L. Chen, G. Nam, X. Liu, J. Cho, Adv. Energy Mater. 8 (2018) 1801478.
[33] L. Bu, N. Zhang, S. Guo, X. Zhang, J. Li, J. Yao, T. Wu, G. Lu, J.-Y. Ma, D. Su, X. Huang, Science 354 (2016) 1410–1414.
[34] L. Wang, Z. Zeng, W. Gao, T. Maxson, D. Raciti, M. Giroux, X. Pan, C. Wang, J. Greeley, Science 363 (2019) 870–874.
[35] J. Zhu, M. Xiao, P. Song, J. Fu, Z. Jin, L. Ma, J. Ge, C. Liu, Z. Chen, W. Xing, Nano Energy 49 (2018) 23–30.
[36] C. Tang, B. Wang, H.F. Wang, Q. Zhang, Adv. Mater. 29 (2017).
[37] J. Kibsgaard, T.F. Jaramillo, F. Besenbacher, Nat. Chem. 6 (2014) 248.
[38] E.J. Popczun, C.G. Read, C.W. Roske, N.S. Lewis, R.E. Schaak, Angew. Chem. Int. Ed. 53 (2014) 5427–5430.
[39] J. Kibsgaard, T.F. Jaramillo, Angew. Chem. Int. Ed. 53 (2014) 14433–14437.
[40] H.-W. Liang, S. Brüller, R. Dong, J. Zhang, X. Feng, K. Müllen, Nat. Commun. 6 (2015) 7992.
[41] A. Laursen, K. Patraju, M. Whitaker, M. Retuerto, T. Sarkar, N. Yao, K. Ramanujachary, M. Greenblatt, G.C. Dismukes, Energy Environ. Sci. 8 (2015) 1027–1034.
[42] J. Xu, T. Liu, J. Li, B. Li, Y. Liu, B. Zhang, D. Xiong, I. Amorim, W. Li, L. Liu, Energy Environ. Sci. 11 (2018) 1819–1827.
[43] J. Mahmood, F. Li, S.-M. Jung, M.S. Okyay, I. Ahmad, S.-J. Kim, N. Park, H. Y. Jeong, J.-B. Baek, Nat. Nanotechnol. 12 (2017) 441.
[44] L. Ma, L.R.L. Ting, V. Molinari, C. Giordano, B.S. Yeo, J. Mater. Chem. 3 (2015) 8361–8368.
[45] J.R. McKone, B.F. Sadtler, C.A. Werlang, N.S. Lewis, H.B. Gray, ACS Catal. 3 (2013) 166–169.
[46] Y.-Y. Chen, Y. Zhang, W.-J. Jiang, X. Zhang, Z. Dai, L.-J. Wan, J.-S. Hu, ACS Nano 10 (2016) 8851–8860.
[47] Y. Zheng, Y. Jiao, Y. Zhu, L.H. Li, Y. Han, Y. Chen, M. Jaroniec, S.-Z. Qiao, J. Am. Chem. Soc. 138 (2016) 16174–16181.
[48] H. Li, C. Tsai, A.L. Koh, L. Cai, A.W. Contryman, A.H. Fragapane, J. Zhao, H.S. Han, H.C. Manoharan, F. Abild-Pedersen, J.K. Nørskov, X. Zheng, Nat. Mater. 15 (2015) 48.

Jianbing Zhu received his BS from Beihang University, Beijing in 2010. He obtained his PhD degree in Physical Chemistry from Changchun Institute of Applied Chemistry, Chinses Academy of Sciences in 2016. Then he works as a postdoctoral research fellow in the University of Waterloo, and his research interests focus on the development of non-precious metal electrocatalysts for fuel cells and metal-air batteries.

Dr. Shuang Li received her Ph.D. in 2018 from Institute of Metal Research, Chinese Academy of Sciences. Then she worked as a postdoctoral research fellow in University of Waterloo. Her research interests are mainly focused on microstructure characterization of energy storage materials by using advanced electron microscopy.

Meiling Xiao received her BS from Nanjing Normal University, China, in 2011 and Ph. D degree in Physical Chemistry from Changchun Institute of Applied Chemistry, Chinses Academy of Sciences in 2016. Currently, she works as a postdoctoral research fellow in the University of Waterloo, now her research interests focus on the exploration of earth-abundant materials to replace noble metal materials for electrocatalytic process and the understanding of electrocatalysis mechanism on these novel electrocatalysts.

Xiao Zhao received his Ph.D. degree from Changchun Institute of Applied Chemistry, Chinese Academy of Sciences in 2013. After postdoc at National University of Singapore, He became a Project Assistant Professor at Innovation Research Center for Fuel Cells, the University of Electro-Communications in Tokyo in 2014. His current research interests focus on the understanding of model electrocatalysts by the combination of controllable synthesis, advanced electron microscopy and in-situ X-ray absorption fine structure.

Gaoran Li is currently a postdoctoral researcher in the Department of Chemical Engineering, University of Waterloo, Canada. He received his Ph.D. degree in Chemical Engineering from the College of Chemical and Biological Engineering, Zhejiang University, in 2016. His research interests focus on energy-storage materials for advanced lithium-ion and lithium-sulfur batteries.

Dr. Zhengyu Bai is an associate professor at School of Chemistry and Chemical Engineering at Henan Normal University. She received her Ph.D. in 2010 from Henan Normal University. She received the Distinguished Young Investigator Awards at the 4th International Conference on Electrochemical Energy Science and Technology 2018 (EEST 2018). Her research is focused on new green energy nanomaterials, such as nanostructured electrocatalysts for fuel cell and metal-air batteries. Dr. Bai has published over 80 peer-reviewed journal articles. She is also listed as an inventor on 25 national patents, with 8 patents licensed in China.

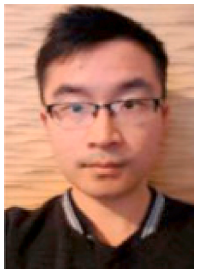

Matthew Li is pursuing his Ph.D. study at the University of Waterloo in the Department of Chemical Engineering. He is currently conducting his research work at Argonne National Laboratories as a visiting student. His research interest mainly focuses on nanomaterials for application in energy storage systems such as lithium-ion and lithium sulfur batteries.

Yongfeng Hu, PhD, Senior Scientist at the Canadian Light Source. His expertise is with the development of synchrotron-based techniques, including the beamline and endstations. His research interest is the applications of these techniques, with a focus on the in-situ studies of energy materials and environmental research.

Dr Renfei Feng is a Senior Scientist responsible for a hard X-ray microprobe facility at the Canadian Light Source – the national synchrotron research center in Canada. He is also an Adjunct Professor in University of Saskatchewan, Canada. He obtained his PhD degree in 1993 in Atomic and Molecular Physics. His current research interests focus on advanced synchrotron instrumentation and applications, including the techniques of X-Ray spectroscopies, imaging, diffraction, and their applications in the materials sciences, environmental sciences, and life sciences.

Wenwen Liu is now pursuing his Ph.D. degree in Department of Chemical Engineering under the supervision of Prof. Aiping Yu at the University of Waterloo. His research mainly focuses on the design and construction of advanced functional materials and their applications in electrochemical energy storage and electrocatalysis.

Rui Gao received his B.S. degree in 2013 from Hengshui University. He obtained his PhD degree in Materialogy from University of Chinese Academy of Sciences (UCAS) and then joined Dr. Chen's group in University of Waterloo as a postdoctor fellow. He is mainly focused on energy storage materials and developing in-situ characterization methods.

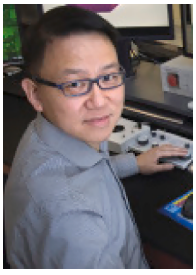

Dr. Dong Su is a Professor at Institute of Physics (IOP), Chinese Academy of Sciences (CAS). He is also an adjunct professor in the Department of Materials Science and Engineering at Stony Brook University since 2011. He got his B.S. in 1998 from Nanjing University. He got his Ph.D in condensed matter physics in 2003, from Nanjing University and IOP, CAS. After doing postdoc in EPFL, Switzerland, University of Illinois at Urbana-Champaign, and Arizona State University, he joined Brookhaven National Laboratory in 2008 as an assistant scientist in Center for Functional Nanomaterials (CFN). He has been through the rank and was promoted to scientist with continuing appointment in 2015 and in 2019, he was the group leader of electron microscopy in CFN. Dr. Dong Su has published more than 300 papers in peer-reviewed journals with citation >19,000.

Dr. Aiping Yu is Professor at University of Waterloo. Her research interests focus on development, processing and functionalization of nanostructured carbon materials, along with their application as electrode materials in high performance supercapacitors. She has published over 140 refereed journal papers, 3 book chapters and one book. These publications have received over 12000 citations. She holds 7 patents and provisional patents for nanomaterials or device development, and 2 of these have been licensed to industry.

Dr. Zhongwei Chen is Canada Research Chair Professor in Advanced Materials for Clean Energy at University of Waterloo, fellow of the Royal Society of Canada and fellow of the Canadian Academy of Engineering. His research interests are in the development of advanced energy materials for metal-air batteries, lithium ion batteries and fuel cells. He has published 1 book, 7 book chapters and more than 300 peer reviewed journal articles with over 28,000 citations with H-index 81 (Google Scholar). He is also listed as inventor on 15 US/international patents, with several licensed to companies in USA and Canada. He was recipient of the 2016 E. W. R Steacie Memorial Fellowship, which followed shortly upon several other prestigious honors, including the Ontario Early Researcher Award, an NSERC Discovery Supplement Award, the Distinguished Performance and the Research Excellence Awards from the University of Waterloo.